

On the non-detection of solar-like pulsations in the host star GJ 504 observed by TESS

MARIA PIA DI MAURO,¹ RAFFAELE REDA,^{2,1} SAVITA MATHUR,^{3,4} RAFAEL A. GARCÍA,⁵ DEREK L. BUZASI,⁶ ENRICO CORSARO,⁷ OTHMAN BENOMAR,^{8,9}
LUCÍA GONZÁLEZ CUESTA,^{3,4} KEIVAN G. STASSUN,^{10,11} SERENA BENATTI,¹² VALENTINA D'ORAZI,^{13,14} LUCA GIOVANNELLI,^{2,1} AND DINO MESA¹³

¹INAF-IAPS, Istituto di Astrofisica e Planetologia Spaziali Via del Fosso del Cavaliere 100 00133 Roma, Italy

²Dipartimento di Fisica, Università di Roma Tor Vergata, Via della Ricerca Scientifica 1, 00133 Roma, Italy

³Instituto de Astrofísica de Canarias (IAC), 38205 La Laguna, Tenerife, Spain

⁴Universidad de La Laguna (ULL), Departamento de Astrofísica, E-38206 La Laguna, Tenerife, Spain

⁵AIM, CEA, CNRS, Université Paris-Saclay, Université de Paris, Sorbonne Paris Cité, F-91191 Gif-sur-Yvette, France

⁶Dept. of Chemistry & Physics, Florida Gulf Coast University, 10501 FGCU Blvd. S., Fort Myers, FL 33965 USA

⁷INAF-Astrophysical Observatory of Catania, Via S. Sofia 78 95123 Catania, Italy

⁸National Astronomical Observatory of Japan, Mitaka, Tokyo, Japan

⁹Center for Space Science, New York University Abu Dhabi, UAE

¹⁰Vanderbilt University, Department of Physics & Astronomy, 6301 Stevenson Center Ln., Nashville, TN 37235, USA

¹¹Vanderbilt Initiative in Data-intensive Astrophysics (VIDA), 6301 Stevenson Center Lane, Nashville, TN 37235, USA

¹²INAF - Osservatorio Astronomico di Palermo, Piazza del Parlamento 1, 90134 Palermo, Italy

¹³INAF Osservatorio Astronomico di Padova, vicolo dell'Osservatorio 5 35122, Padova Italy

¹⁴School of Physics and Astronomy, Monash University, Clayton, VIC 3800, Australia

(Received; Accepted)

Submitted to ApJ

ABSTRACT

We present the results of the analysis of the photometric data collected in long-cadence mode by the Transiting Exoplanet Survey Satellite (TESS) for GJ 504, a well studied planet-hosting solar-like star, whose fundamental parameters have been largely debated during the last decade. Several attempts have been made by the present authors to isolate the oscillatory properties expected on this main-sequence star with mass $M = (1.28 \pm 0.07)M_{\odot}$, radius $R = (1.38 \pm 0.2)R_{\odot}$ and age ≤ 2.6 Gyr, as predicted by theoretical models. We found only a marginal hint of presence of pulsations around $\approx 2000 \mu\text{Hz}$ and we report only with low statistical significance a large separation $\Delta\nu = (85.0 \pm 3.6)\mu\text{Hz}$. The suppression of the amplitude of the acoustic modes can be explained by the high level of magnetic activity revealed for this target, not only by the study of the photometric light-curve, but also by the analysis of three decades available of Mount Wilson spectroscopic data. In particular, our new measurements of the stellar rotational period $P_{rot} \approx 12.5$ d and of the main principal magnetic cycle of ≈ 12 a allow us to locate this star in the early main sequence phase of its evolution during which the chromospheric activity is dominated by the superposition of several cycles before the transition to the phase of magnetic-braking shutdown with subsequent decrease of the magnetic activity.

Keywords: stars: oscillations, stars: interiors, stars: individual (GJ 504), stars: solar-type

1. INTRODUCTION

Over the last decade, thanks to the successful photometric space missions, CoRoT (Convection, Rotation, and Transits Baglin et al. 2006) and Kepler/K2 (Borucki et al. 2010)

mainly conceived for exoplanets, but extremely suitable for detection of stellar pulsations, asteroseismology has produced an extraordinary revolution in astrophysics (e.g. Beck et al. 2012; Bedding et al. 2011; Silva Aguirre et al. 2015; Stello et al. 2016). This unveiled a wealth of results on the physical properties of stars over a large part of the H-R diagram and mostly for solar-like stars, which exhibit pulsations excited by near-surface turbulent convection, as it happens in the Sun.

48 The extreme photometric precision made these missions
 49 spectacularly successful also in their primary goal: the de-
 50 tection and characterization of extra-solar planetary systems
 51 by using the transit technique (Borucki et al. 2013). Thus, in
 52 recent years a flood of very high-quality data has been col-
 53 lected and the search for new worlds is in progress and we are
 54 living exciting times in this respect. Despite the incredible ef-
 55 fort in refining observational and post-processing techniques,
 56 our interpretation and comprehension of planetary systems
 57 architecture, formation and evolution mechanisms heavily re-
 58 lies on the accuracy of the inferred characteristics of the host
 59 stars and the effects on their planets (Van Eylen et al. 2014;
 60 Borucki et al. 2013; Huber et al. 2013; Chaplin et al. 2013).
 61 This often represents a significant challenge, especially for
 62 isolated field stars (Soderblom et al. 2014).

63 The most recently launched NASA space mission Transiting
 64 Exoplanet Survey Satellite, TESS (Ricker et al. 2014),
 65 is poised to continue the synergy between asteroseismology
 66 and exoplanet science, enlarging the held of asteroseismic
 67 inference to full-sky. Indeed, with the original high-cadence
 68 mode of 120-s (Nyquist frequency of 4166 μ Hz) used during
 69 the first two years of its main mission and the newer fast ca-
 70 dence of 20-s that started during the extended mission, TESS
 71 should be able to detect oscillation in many main-sequence
 72 solar-like stars in spite of their low intrinsic amplitudes of
 73 parts-per million (García & Ballot 2019).

74 According to the TESS Asteroseismic Target List
 75 (Schofield et al. 2019; Campante et al. 2016), thousands of
 76 main-sequence and subgiant solar-like stars should show de-
 77 tectable modes. So far, signatures of such oscillations have
 78 been detected only in a handful of solar-like stars (e.g., Gan-
 79 dolfi et al. 2018; Huber et al. 2019; Chontos et al. 2020; Met-
 80 calfe et al. 2020; Addison et al. 2021; Metcalfe et al. 2021).
 81 Recently, Huber et al. (2021) compared the power spectra
 82 of three stars observed by TESS with both cadences of 2-
 83 min and 20-s. While the modes were barely visible with the
 84 2-min cadence, the faster cadence drastically increased the
 85 signal-to-noise ratio allowing the characterization of the in-
 86 dividual modes. Part of this improvement could be explained
 87 by the difference of the cosmic-ray rejection applied to both
 88 cadences. However, the difficulties to detect the oscillation
 89 modes could also be due to the properties of the stars.

90 The non-detection of modes has been investigated also in
 91 many stars observed by the *Kepler* mission. For solar-like
 92 stars, the usual explanation is the surface magnetic activity of
 93 the star (e.g., Chaplin et al. 2011a) as it is known that a high
 94 level of magnetic activity can reduce the amplitude of the
 95 modes (García et al. 2010; Kiefer et al. 2017; Santos et al.
 96 2018) Nevertheless this is not the only culprit as shown in
 97 Mathur et al. (2019a). Indeed metallicity or binarity can also
 98 have an impact on the amplitude of the modes (Gaulme et al.
 99 2020).

100 Here, we present the result of the analysis of the solar-type
 101 star GJ 504 (spectral type G0), which was observed by the
 102 TESS mission for 27 days during sector 23 from March 18,
 103 2020 to April 16, 2020 using 2 minutes cadence mode. Fur-
 104 thermore, spectroscopic observations from the Mount Wilson
 105 Observatory are also studied to better characterize the surface
 106 magnetic activity of the star.

107 GJ 504 is considered a very interesting case study, claimed
 108 to host a sub-stellar companion whose nature is strongly
 109 debated. Nevertheless, asteroseismology might provide the
 110 only powerful mean to dissolve any doubts about the evolu-
 111 tionary state of this target and hence on the identity of the
 112 secondary object. In fact, the detection of typical signatures
 113 of solar-like oscillations in the power spectrum would define
 114 with good accuracy the age and all the physical parameters
 115 of this low-mass star. There are many methods to estimate
 116 the age of a single star: empirical indicators such as stel-
 117 lar activity and gyrochronology which link rotation to age
 118 (e.g., Skumanich 1972; Barnes 2007; Mamajek & Hillen-
 119 brand 2008); photospheric lithium abundance; comparison
 120 of stellar model isochrones with observed classical param-
 121 eters. However the accuracy that can currently be reached by
 122 using all these methods is not satisfactory, not only because
 123 of the large errors in the estimates, but also because better
 124 precision and accuracy can be reached only by using seismic
 125 diagnostics (see, e.g., Metcalfe et al. 2010; Lebreton et al.
 126 2014; Lebreton & Goupil 2014).

127 This paper is organized in the following sections: Section
 128 2 introduces the reader to the target presenting the spectro-
 129 scopic fundamental parameters and the theoretical predic-
 130 tions deduced by means of stellar evolutionary models and
 131 asteroseismic scaling laws; Section 3 presents the observa-
 132 tions and the data calibration used in this work; in Section
 133 4, we study the surface rotation and magnetic activity of the
 134 this star; in Section 5, we describe the search for solar-like
 135 oscillations; Section 6 discusses the reasons for the non de-
 136 tection of solar-like oscillations and presents the attempt to
 137 characterize the structure of this star; Section 7 shows the
 138 conclusions.

139 2. THE SOLAR-LIKE STAR GJ 504

140 2.1. An intriguing case

141 During the last 25 years, several dedicated space mis-
 142 sions, together with great developments in observational
 143 techniques, have allowed huge progresses in the search for
 144 new worlds outside the solar system. In particular, besides
 145 statistics, several hundreds of bright stars have been moni-
 146 tored and multi-wavelengths data collected in order to under-
 147 stand and characterize the formation and the evolution of the
 148 already discovered planetary systems.

149 A controversial case still debated today is represented by
 150 the solar-type star GJ 504 (HD 115383, TIC 397587084), a

151 G0-type star with $T_{\text{eff}} \approx 6200 \text{ K}$, which appears to be a little
 152 more massive than the Sun (Kuzuhara et al. 2013; D’Orazi
 153 et al. 2017), with a rotational period $P_{\text{rot}} = 3.329$ days, aver-
 154 age of the values reported by Messina et al. (2003) and Don-
 155 ahue et al. (1996). In 2013, by exploiting high-contrast near-
 156 IR and L-band observations, Kuzuhara et al. (2013) iden-
 157 tified a Jovian planet orbiting this star. Employing the gy-
 158 rochronology technique, based on the stellar chromospheric
 159 activity indexes (as given by the Ca II H and K emission
 160 lines) and on X-ray observations (the star is included in the
 161 ROSAT catalogue), Kuzuhara et al. (2013) estimated the age
 162 of GJ 504 to be $\text{Age} = 160_{-60}^{+350}$ Myr. Under this assump-
 163 tion, the comparison of observational data with theoretical
 164 models implies that the mass of the sub-stellar companion
 165 (named GJ 504b) should be $M_{\text{GJ 504b}} = 4_{-1.0}^{+4.5} M_{\text{Jup}}$. According
 166 to Kuzuhara et al. (2013), the measured characteristics make
 167 GJ 504b a very interesting object because it represents the
 168 first example of giant planet on a wide orbit around a solar-
 169 type star. Moreover, the planet appears to be significantly
 170 cool ($T_{\text{eq}} = 510_{-20}^{+30} \text{ K}$), with an almost cloud-free atmosphere
 171 due to its blue color ($J - H = -0.23$) and, as reported by Jan-
 172 son et al. (2013), represents the first known extrasolar planet
 173 with methane-dominated atmosphere (T-type).

174 However, few years later the young age of GJ 504 has been
 175 disproved by Fuhrmann & Chini (2015): thanks to evidences
 176 arising from high-resolution and high-quality spectra. In fact,
 177 the authors derived a stellar gravity of $\log g = 4.23$ dex (from
 178 the Hipparcos parallax and adopting spectroscopic tempera-
 179 ture), which results to be not compatible with a stellar age of
 180 few hundreds Myr. This gravity estimate is also in agreement
 181 with the value of $\log g = 4.17$ dex previously determined
 182 in Fuhrmann (2004), based on the spectral fitting of Mg Ib
 183 lines and several independent spectroscopic studies and po-
 184 sition of the star in the color-magnitude diagram (see, e.g.,
 185 da Silva et al. 2012). This picture implies that GJ 504 should
 186 be a star with approximately the solar age and, as a conse-
 187 quence, the companion has to be identified as a brown dwarf
 188 ($M_{\text{GJ 504b}} \sim 25 M_{\text{Jup}}$) rather than a giant planet. In order to
 189 explain the relatively high rotation period and chromospheric
 190 activity level of the host star, and reconcile isochronal ages
 191 with direct indicators, Fuhrmann & Chini (2015) invoked a
 192 merging event. GJ 504 might have engulfed a sub-stellar
 193 companion that is responsible for speeding up the rotational
 194 velocities and accounts for the enhanced activity levels.

195 D’Orazi et al. (2017), reassessing the properties of GJ 504,
 196 have found that the surface gravity of the star implies an evo-
 197 lutionary stage obtained by the isochrones comparison which
 198 suggests an age range between 1.8-3.5 Gyr (most probable
 199 age ≈ 2.5 Gyr). To reconcile all the age indicators and to
 200 explain the high level of activity, also these authors suggest
 201 a merging scenario (more recent than 200 Myr) with a very
 202 close hot Jupiter companion.

203 The system has been recently revisited by Bonnefoy et al.
 204 (2018) by using interferometric, radial-velocity, and high-
 205 contrast imaging observations. They found an interferomet-
 206 ric radius of $R = (1.35 \pm 0.04)R_{\odot}$ for GJ 504, which is com-
 207 patible with two isochronal age ranges (21 ± 2) Myr and
 208 (4.0 ± 1.8) Gyr. According to this work, the mass of GJ 504b
 209 is expected to be $M_{\text{GJ 504b}} = 1.3_{-0.3}^{+0.6} M_{\text{Jup}}$ for the young age
 210 case and $M_{\text{p}} = 23_{-9}^{+10} M_{\text{Jup}}$ for the old one.

211 Therefore, the evolutionary stage and the age of GJ 504
 212 is still an open problem with no clear solution to date. This
 213 uncertainty closely concerns the mass estimation of the star’s
 214 companion, which could be a Jovian planet or a brown-dwarf.
 215 In addition, Skemer et al. (2016), through a photometric
 216 study, suggested for GJ 504b a higher metallicity ($[M/H]_{\text{p}} \approx$
 217 $+0.6$) with respect to the host star ($[Fe/H]_{\star} \approx +0.1 - 0.3$),
 218 adding to this system another element of interest.

219 For all the above mentioned reasons the GJ 504 system
 220 constitutes an intriguing case which, deserves to be carefully
 221 studied, with the aim of shedding light on the age of the star
 222 and, accordingly, on the nature of the sub-stellar companion.

2.2. Fundamental parameters

224 In order to properly characterize this star we performed
 225 an analysis of the broadband Spectral Energy Distribution
 226 (SED) together with the *Gaia* EDR3 (*Gaia* Collaboration
 227 2018) parallax measurement following the procedures de-
 228 scribed in Stassun & Torres (2016), Stassun et al. (2017), and
 229 Stassun et al. (2018). The input parameters and the obtained
 230 results are summarized in Table 1. We employed the *UBV*
 231 magnitudes from Mermilliod (2006), the $B_T V_T$ magnitudes
 232 from *Tycho-2*, the Strömgen *uvby* magnitudes from Paun-
 233 zen (2015), the *JHK_S* magnitudes from 2MASS, the W1–
 234 W4 magnitudes from *WISE*, and the FUV magnitude from
 235 *GALEX*. The available photometry, all together, spans the full
 236 stellar SED over the wavelength range $0.2 - 22 \mu\text{m}$ (Fig. 1).

238 We performed a fit using Kurucz stellar atmosphere mod-
 239 els, with the T_{eff} , $\log g$, $[Fe/H]$, and $v \sin i$ taken from the
 240 spectroscopic analysis of D’Orazi et al. (2017). The re-
 241 maining parameter is the extinction (A_V), which we fixed
 242 to be zero due to the star’s proximity. The resulting fit is
 243 shown in Fig. 1, obtained with a reduced $\chi^2 = 1.9$. Inte-
 244 grating the model SED gives the bolometric flux at Earth of
 245 $F_{\text{bol}} = (2.096 \pm 0.024) \cdot 10^{-7} \text{ erg s}^{-1} \text{ cm}^{-2}$. Taking the F_{bol}
 246 and T_{eff} together with the *Gaia* parallax, with no adjustment
 247 for systematic parallax offset (see, e.g., Stassun & Torres
 248 2021), gives the stellar radius as $R_{\star} = (1.227 \pm 0.012)R_{\odot}$.
 249 The F_{bol} and parallax also yield directly the bolometric lumi-
 250 nosity, $L_{\star} = (2.01 \pm 0.03)L_{\odot}$.

251 The empirical stellar radius determined above affords an
 252 opportunity to estimate the stellar mass empirically as well,
 253 via the spectroscopically determined surface gravity, obtain-
 254 ing $M_{\star} = (1.07 \pm 0.17) M_{\odot}$. This value is consistent with

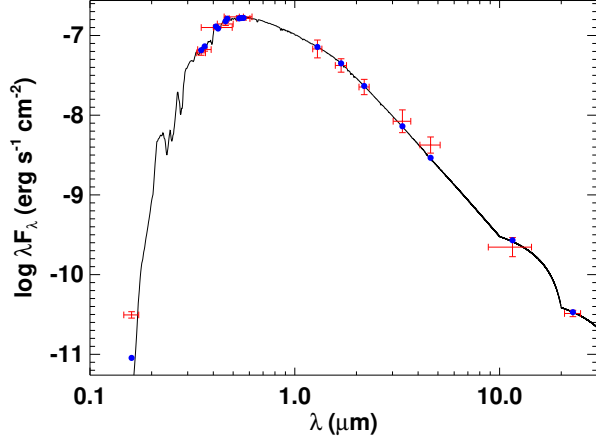


Figure 1. Spectral energy distribution. Red symbols represent the observed photometric measurements, where the horizontal bars represent the effective width of the pass-band. Blue symbols are the model fluxes from the best-fit Kurucz atmosphere model (black).

Table 1. The fundamental parameters of GJ 504 (TIC 397587084).

Basic Properties	
TESS Magnitude	4.6552 ± 0.0073^a
π (mas)	57.0186 ± 0.2524^b
Spectroscopic parameters ^c	
T_{eff} (K)	6205 ± 20
[Fe/H] (dex)	0.22 ± 0.04
$v \sin i$ (km s ⁻¹)	2.8 ± 1.6
log g (dex)	4.29 ± 0.07
SED results	
F_{bol} (erg s ⁻¹ cm ⁻²)	$(2.10 \pm 0.02) \cdot 10^{-8}$
L_{\star}/L_{\odot}	2.01 ± 0.03
M_{\star}/M_{\odot}	1.07 ± 0.17
R_{\star}/R_{\odot}	1.227 ± 0.012
P_{SED} (days)	2.4 ± 1.3
Age_{\star} (Gyr)	0.2 ± 0.2

Notes:

^a Adopted from the TESS Input Catalog (Stassun et al. 2019).

^b Gaia measurement (see Gaia Collaboration 2018)

^c Determined by spectroscopic observations (see D’Orazi et al. 2017)

that estimated via the eclipsing-binary based relations of Torres et al. (2010).

Using the activity-age relations of Mamajek & Hillenbrand (2008), we obtained from R'_{HK} and the star’s $B - V$ color, an age of $\text{Age}_{\star} = (0.2 \pm 0.2)$ Gyr and a rotational period for

the star of $P_{\text{SED}} = (2.4 \pm 1.3)$ days which is consistent with previous findings of 3.3 days (Donahue et al. 1996; Messina et al. 2003; Wright et al. 2011).

2.3. The seismic properties and the asteroseismic prediction by scaling laws

The properties of a solar-like pulsating star can be described by adopting the asymptotic development by Tassoul (1980), which predicts that the oscillations excited in main-sequence stars are acoustic modes (p modes) with frequencies $\nu_{n,l}$ characterized by radial order n and harmonic degree l , which for $l \leq n$ should satisfy the following approximation:

$$\nu_{n,l} \sim \Delta\nu \left(n + \frac{l}{2} + \epsilon \right), \quad (1)$$

where ϵ is a function of frequency and depends on the properties of the surface layers and $\Delta\nu$, known as the large frequency separation, is the inverse of the sound travel time across the stellar diameter:

$$\Delta\nu = \left(2 \int_0^R \frac{dr}{c} \right)^{-1}, \quad (2)$$

where c is the local speed of sound at radius r and R is the photospheric stellar radius. Hence, according to the theory, the solar-like oscillations spectrum of GJ 504 should show a series of equally spaced peaks separated by $\Delta\nu$ between p modes of same degree l and adjacent n :

$$\Delta\nu \simeq \nu_{n+1,l} - \nu_{n,l} \equiv \Delta\nu_l. \quad (3)$$

In addition, the power spectra of this target should show another series of peaks, whose separation $\delta\nu_l$ is known as the small separation:

$$\delta\nu_l \equiv \nu_{n,l} - \nu_{n-1,l+2} \quad (4)$$

which is sensitive to the chemical composition gradient in the central regions of the star and hence to its evolutionary state. Thus, the determination of the large and small frequency separations from the observed oscillation spectrum can directly provide asteroseismic inferences on the mass and the age of GJ 504 (Christensen-Dalsgaard 1988).

The observed oscillation power spectrum of the solar-like stars is characterized by a typical Gaussian like envelope and the frequency of maximum oscillation power is usually indicated by ν_{max} . As conjectured by Brown et al. (1991), the frequency ν_{max} can be related to the acoustic cutoff frequency ν_{ac} , which defines the upper boundary of the p mode resonant cavities:

$$\nu_{\text{max}} \propto \nu_{\text{ac}} \propto g T_{\text{eff}}^{-1/2}, \quad (5)$$

Thus, according to Eq. 5, the frequency ν_{max} carries information on the physical conditions in the near-surface layers

of the star. Thus, as it has been well demonstrated both theoretically (Chaplin et al. 2008; Belkacem et al. 2011) than observationally (Bedding & Kjeldsen 2003; Stello et al. 2008; Bedding 2014), as a solar-type star evolves, its oscillation spectrum moves towards lower frequencies due to the decrease of the surface gravity.

In order to extract a rough estimate of the asteroseismic parameters of the star to be adopted as guess values for the oscillation analysis, it is possible to assume well proved scaling-laws as those provided by (see, e.g., Brown et al. 1991; Kjeldsen & Bedding 1995), and by Huber et al. (2011). These relations, which have been typically calibrated on large samples of main-sequence stars, offer the possibility to predict the range of frequencies where the excess of power for a given solar-like star will manifest. By assuming the relation by Kjeldsen & Bedding (1995); Kjeldsen et al. (2008), we calculated the value of the expected maximum amplitude of oscillation A_{\max} and the frequency at the maximum amplitude ν_{\max} , using the observed surface gravity g and the effective temperature T_{eff} of the star. By using scaling relations and corrections by Campante et al. (2016) we obtained a value for the expected maximum amplitude in the range $A_{\max} = (2.51 - 2.95)$ ppm depending on which input spectroscopic parameters are assumed.

Table 2 shows the results for the expected ν_{\max} computed assuming spectroscopic measurements published by different authors. Except for the ν_{\max} from the stellar parameter of Valenti & Fischer (2005), who reported a high surface gravity, all the expected values for the frequency of maximum oscillation lie in the range (1800-2300) μHz . Thus, if there is an excess of power due to oscillations in the GJ 504 spectrum, we expect to find it in this range of frequencies.

2.4. Theoretical prediction by evolutionary models

Given the observed fundamental parameters collected in Table 1, it is also possible to face the theoretical challenge to infer the structural properties of GJ 504 and predict its detailed oscillation spectrum by constructing stellar evolutionary models which satisfy the observational constraints.

We produced theoretical structure models for the star by using the ASTEC evolutionary code (Christensen-Dalsgaard 2008a) by varying the mass and the composition in order to match the atmospheric parameters available. The resulting evolutionary tracks characterized by fixed mass M and initial chemical composition have been calculated with the OPAL 2005 equation of state (Rogers & Nayfonov 2002), OPAL opacities (Iglesias & Rogers 1996), and the NACRE nuclear reaction rates (Angulo et al. 1999). Convection was treated according to the mixing-length formalism (MLT) (Böhm-Vitense 1958) and defined through the parameter $\alpha = \ell/H_p$,

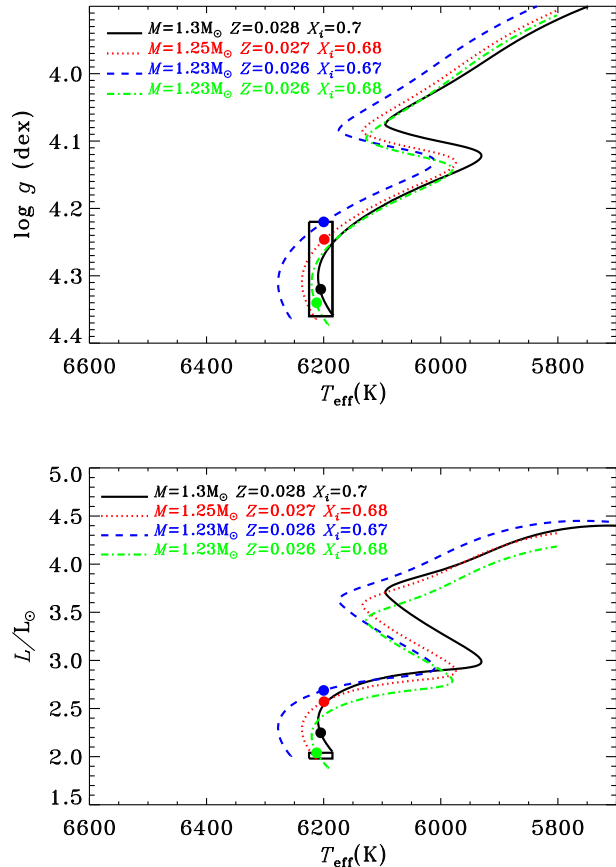


Figure 2. Evolutionary tracks plotted in two plans of the H-R diagram calculated for different values of the mass and the metallicity, while all the other parameters are fixed. The initial hydrogen abundance is X_i , and the mixing-length coefficient is $\alpha = 1.8$. The rectangle defines the one-sigma error box for the observed gravity and effective temperature. Coloured dots indicate the position of the four structure models (see Table 6.2) which best reproduce the observations of GJ 504.

where H_p is the pressure scale height and α is assumed to be 1.8. The initial heavy-element mass fraction Z in respect to the abundance of the hydrogen X has been calculated from the iron abundance given in Table 1 using the relation $[\text{Fe}/\text{H}] = \log(Z/X)_s - \log(Z/X)_\odot$, where $(Z/X)_s$ is the value at the stellar surface and the solar value was taken to be $(Z/X)_\odot = 0.0245$ (Grevesse & Noels 1993).

Fig. 2 shows a series of evolutionary tracks obtained for different masses and fixed initial composition, plotted in two H-R diagrams, representing respectively the effective temperature-gravity plane and the effective temperature-luminosity plane. The present evolutionary models do not include additional effects such as overshooting, settling of heavy elements and rotation.

The location of the star in the H-R diagram identifies GJ 504 as being at the beginning of the main sequence phase.

Table 2. Predictions for the frequency of maximum oscillation computed assuming spectroscopic data obtained by different authors .

T_{eff}	$\log g$	ν_{max}	Reference
(K)	(cm/s ²)	(μ Hz)	
6205 \pm 20	4.29 \pm 0.07	2096 \pm 338	D’Orazi et al. (2017)
5978 \pm 60	4.23 \pm 0.10	1860 \pm 428	Fuhrmann & Chini (2015)
6130 \pm 48	4.33 \pm 0.10	2312 \pm 533	Maldonado et al. (2015)
6185 \pm 51	4.30 \pm 0.07	2148 \pm 346	Battistini & Bensby (2015)
5995 \pm 41	4.24 \pm 0.02	1900 \pm 88	Ramírez et al. (2013)
6012 \pm 100	4.30 \pm 0.20	2179 \pm 100	Mishenina et al. (2013)
6234 \pm 25	4.60 \pm 0.02	4269 \pm 197	Valenti & Fischer (2005)

In fact, only a small percentage of the hydrogen fuel, indicated by X_c in Table 6.2, has been already converted into helium. The uncertainty in the observed value of Z_s introduces an uncertainty in the determination of the stellar mass whose value, considering only the observed spectroscopic parameters, seems to be limited to the range $M = (1.28 \pm 0.07)M_\odot$ hence slightly more massive than the Sun, in agreement with the value predicted by SED analysis (see Section 2.2). The stellar radius appears $R = (1.38 \pm 0.20)R_\odot$, a value which is in perfect agreement with the interferometric radius measured by Bonnefoy et al. (2018).

The age of this star, as obtained from the evolutionary models, can be estimated in the range 0.0 – 2.6 Gyr, hence younger than the Sun, so that the convective envelope should appear still quite shallow with a depth not larger than $D_{cz} \approx 0.16R$. Thus, we confirm that GJ 504 is a very young star as supposed by Kuzuhara et al. (2013), while our stellar structure models do not show a star of solar age as supposed by Fuhrmann & Chini (2015); Bonnefoy et al. (2018).

In order to predict the observed pulsational scenario of GJ 504, we used the ADIPLS package (Christensen-Dalsgaard 2008b) to compute theoretical adiabatic oscillation frequencies for all the structure models satisfying the spectroscopic constraints. The theoretical result show that the oscillation modes expected to be visible in this star should be $l = 0, 1, 2, 3$ pure acoustic modes with frequencies in the range approximately between (1500 – 3500) μ Hz while the theoretical large separation calculated by linear fit over the asymptotic relation for the radial mode frequencies appear to be $\Delta\nu = (98 \pm 13)\mu$ Hz.

Among all the possible computed structure models, we selected four models chosen in order to best-fit the observed effective temperature, the metallicity and the gravity (Table 1) and with location in the HR diagram shown by coloured dots (see Fig. 2).

In Table 3 we give a comprehensive set of physical properties for the four different models of GJ 504. In particular

Table 3. Main parameters for four best-fit structure models of GJ 504.

	Model 1	Model 2	Model 3	Model 4
M/M_\odot	1.23	1.23	1.25	1.30
Age (Gyr)	0.66	2.46	2.19	0.74
T_{eff} (K)	6212	6200	6200	6205
$\log g$ (dex)	4.34	4.22	4.25	4.32
R/R_\odot	1.23	1.42	1.38	1.30
L/L_\odot	2.04	2.69	2.57	2.25
Z_s	0.026	0.026	0.027	0.028
X_s	0.68	0.67	0.68	0.7
X_c	0.58	0.29	0.35	0.59
[Fe/H]	0.19	0.20	0.21	0.21
r_{cz}/R	0.840	0.837	0.846	0.846
α_{MLT}	1.8	1.8	1.8	1.8
$\Delta\nu$ (μ Hz)	109.6	87.8	90.9	104.5

NOTE— M/M_\odot is the mass of the star, T_{eff} is the effective temperature, $\log g$ is the surface gravity, R/R_\odot is the surface radius, L/L_\odot is the luminosity, Z_s is the surface heavy-element abundance, X_s is the surface hydrogen abundance, X_c is the hydrogen abundance in the core, [Fe/H] is the iron abundance, r_{cz} is the location of the base of the convective region, α_{MLT} is the mixing-length parameter and $\Delta\nu$ is the large separation obtained from the theoretical pulsational frequencies.

Model 1 has been chosen in order to match within 1σ also the luminosity obtained by the SED technique (see Table 1).

We expect to be able to distinguish among the different models of this target by measuring at least the large separation in the observed oscillation spectrum.

3. OBSERVATIONS AND DATA PREPARATION

411 GJ 504 was observed by TESS during 27 consecutive days
 412 of sector 23 from March 18, 2020 to April 16, 2020. In order
 413 to perform the seismic analysis and due to the high-level
 414 of noise of the TESS 120-s cadence data for this star, we
 415 adopted four different strategies to obtain seismically opti-
 416 mized light curves. In such way we ensure that the obtained
 417 results are independent of the methodology applied.

418 The first methodology exploits TESS Science Processing
 419 Operations Center (SPOC, Jenkins et al. 2016) pipeline light
 420 curve, with a cadence of 120 s, available on the MAST
 421 archive¹. This raw light curve shows strong modulations at
 422 low frequency that is filtered out by applying a smoothing
 423 removal process iterated three times. The resultant residuals
 424 are subsequently 3 - σ -clipped to eliminate any outliers as
 425 depicted in panel (a) of Fig. 3.

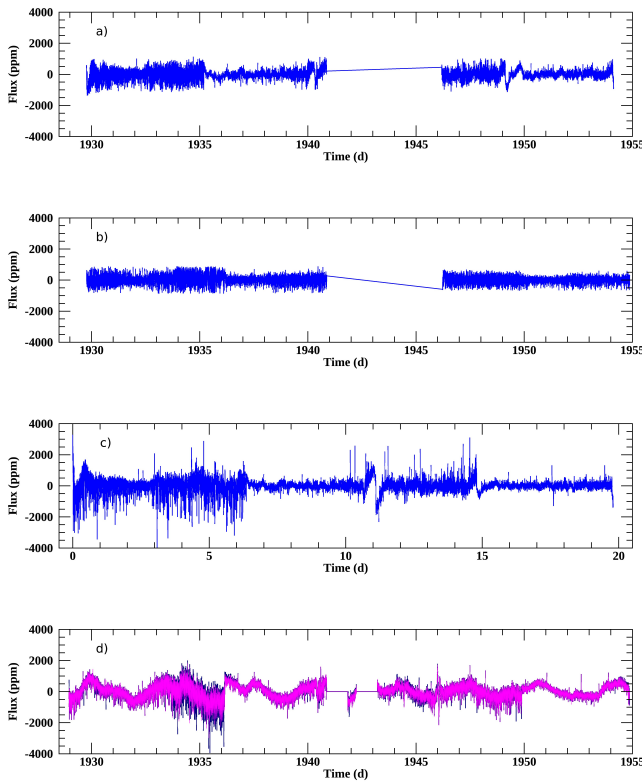


Figure 3. Seismically optimized lightcurves used in this work as explained in Section 3.

426 The second methodology started with the TESS SPOC 120
 427 s cadence target pixel files. We then extracted a time series
 428 for each pixel, rejecting cadences with nonzero quality flags
 429 (see for details the TESS Science Data Products Document²),

¹ <https://archive.stsci.edu/hlsp/tess-spoc>

² <https://archive.stsci.edu/missions/tess/doc/EXP-TESS-ARC-ICD-TM-0014.pdf>

430 and constructed an aperture mask using the procedure de-
 431 scribed in (Buzasi et al. 2016) and (Nielsen et al. 2020). Es-
 432 sentially this process produces a time series with the mini-
 433 mum sum of first differences between successive points. We
 434 then adopted sigma-clipping at the 4σ level combined with
 435 simple gap filling through the use of a piecewise cubic her-
 436 mite interpolating polynomial (PCHIP; as implemented in
 437 Scipy (Jones et al. 2001)). The result is shown in panel (b)
 438 of Fig. 3.

439 The third approach is based on a filtering of the SPOC
 440 lightcurve using two successive Gaussian filters of width 0.25
 441 and 0.125 days. This was done in order to remove long
 442 periodicities and to reduce the noise level. The lightcurve
 443 presents a large gap that could degrade the quality of the
 444 spectrum (window effect). The gap was removed before fil-
 445 tering the lightcurve and the first time stamp was set to zero.
 446 The result is shown in panel (c) of Fig. 3.

447 Finally, the last method started from the target pixel file
 448 to create a larger aperture. In general, light curves obtained
 449 from big apertures are more stable to small instrumental per-
 450 turbations such as the loss of pointing of the satellite or to the
 451 movement of the star during the observations. To build this
 452 larger aperture, contiguous pixels starting from the center of
 453 the target are selected. A new pixel is selected only if the in-
 454 tegrated flux of the pixel has a negative gradient compared to
 455 the previous one (decreasing the flux from the center to avoid
 456 any polluting star) and with an average flux greater than a
 457 given threshold that has been established to 100 e-/s. Once
 458 this is done, an extra pixel at the top and the bottom of the
 459 aperture is added to the 4 central rows, which contain several
 460 saturated pixels. By selecting these extra pixels, the resulting
 461 light curve has smaller dispersion around the mean between
 462 the days 1933.5 and 1936. The final aperture is shown in
 463 Fig. 4. It is important to notice that no significant changes
 464 were found by adding more pixels to the central rows or by
 465 slightly changing the limit threshold of 100 e-/s.

466 To increase the duty cycle, instead of removing all points
 467 with a flag different to zero, we applied two different selec-
 468 tions of the NASA quality flags. We either kept all the points
 469 except the ones with a flag between 2 and 32 (Dark blue curve
 470 in panel (d) of Fig. 3) or between 2 and 512 (magenta curve
 471 in panel (d) of the same figure). We then calibrated the two
 472 resulting lightcurves following (García et al. 2011), remov-
 473 ing outliers, correcting jumps, and drifts. To convert the flux
 474 in parts per million (ppm) and remove the low frequency con-
 475 tribution we used a triangular smooth with a window of half
 476 a day. Except for the big gaps in the middle of the run, all
 477 the rest were interpolated using inpainting techniques with
 478 a multi-scale discrete cosine transform (García et al. 2014a;
 479 Pires et al. 2015). These two lightcurves are longer and with
 480 some more data in the middle of the run than the other three
 481 presented before.

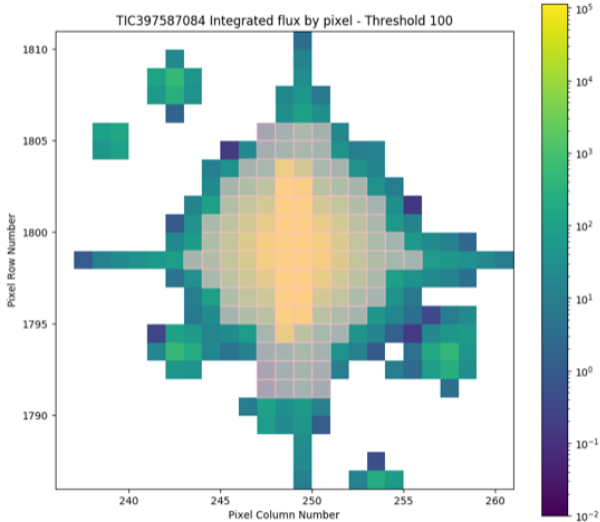


Figure 4. Enlarged mask used in the fourth calibration method described in Sect. 3. The selected pixels are depicted in gray.

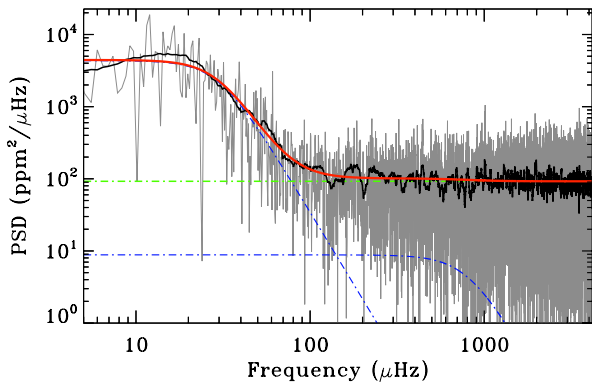


Figure 5. Power spectral density (light gray) with a smoothing overlaid (black curve) of the first seismically optimized lightcurve (shown in panel a) of Fig. 3). The background fit is composed of two Harvey-like profiles (blue curves) and a flat noise level (green curve). The sum of the three components is indicated by the thick red line. No evidence of a Gaussian power excess is found.

In order to do the seismic analysis, the Power Spectral Density (PSD) is computed. As shown in Fig. 5, the PSD is dominated by flat noise above $\sim 200 \mu\text{Hz}$ and a low-frequency slope below $\sim 60 \mu\text{Hz}$. Hence, the background can be characterized by two Harvey components (Harvey 1985) and a flat noise level. As expected, the high-frequency Harvey profile (related to convective noise) has an amplitude of around an order of magnitude smaller than the flat noise component. The low-frequency Harvey profile, with a knee at around $20 \mu\text{Hz}$, is probably related to magnetism and not convection.

GJ 504 is indeed a magnetically active star that was part of a large observational campaign, the HK Project, conducted at the Mount Wilson Observatory (MWO) from 1966 to 1995 with the aim to search for stellar analogs to the solar cycle by

studying stellar chromospheric activity and variability (Wilson 1968, 1978). These measurements are expressed in term of the dimensionless S-index, defined as the ratio of emission in the Ca II H & K line cores to that in two nearby continuum reference bandpasses (for further details see, e.g., Vaughan et al. 1978; Egeland et al. 2017). For this star, within the MWO dataset, about 1342 single measurements are provided in the time interval 1966-1995, allowing us to study its magnetic activity over a time period of nearly 30 years.

4. ROTATION AND MAGNETIC ACTIVITY ANALYSIS

4.1. Rotation

To determine the surface rotation period of GJ 504, a similar methodology as the one applied to the two last lightcurves described in the previous section is employed but this time smoothing the light curve using a triangular filter (double boxcar function). The width of each boxcar is a fifth of the total length. The obtained rotation period, P_{rot} , is independent of the flags removed in the lightcurve because we are interested on the long periods and thus the extra removed peaks with a bad flag do not affect the calculation. To look for P_{rot} , a methodology combining 3 different techniques is used following, e.g., Santos et al. (2019, 2021). The first method performs a time-frequency analysis using a Morlet wavelet (Torrence & Compo 1998). The second utilizes an auto-correlation function (e.g. García et al. 2014b; McQuillan et al. 2014). The third method combines the first two in order to compute the Composite Spectrum (e.g. Ceillier et al. 2016). Hence, a modulation with a periodicity of (3.4 ± 0.25) days is found in the light curve (see Fig. 6).

We also examined the Mount Wilson data to search for a potential rotational periodicity. The data consist of 1342 observations taken between March 1966 and June 1995. Before searching for the presence of a periodicity in the S-index of GJ 504, we visually analyzed the available Mount Wilson data. We noted that 3 measurements taken in 1993, during the same night, are completely outside the mean range of variation (the average MWO S-index for this star is 0.313), with values that are two times larger with respect to all the others. We suspected that such scattered measurements may be the result of an error in the data collection on that night, hence we chose to discard them in the following data analysis of the S-index. We removed the three outliers with S-index values greater than 4σ above the mean, applied a simple linear detrending to the data to remove the lowest-frequency signal, and analyzed the resulting time series using both a DFT and a Lomb-Scargle periodogram. The former results in an estimated rotation period $P_{\text{rot}} = (12.5 \pm 2.8)$ days, while the latter produces (11.8 ± 2.4) days, with uncertainties estimated based on the width of the periodogram peaks. Note that while the Lomb-Scargle peak is significant ($\text{SNR} > 7$) the DFT peak

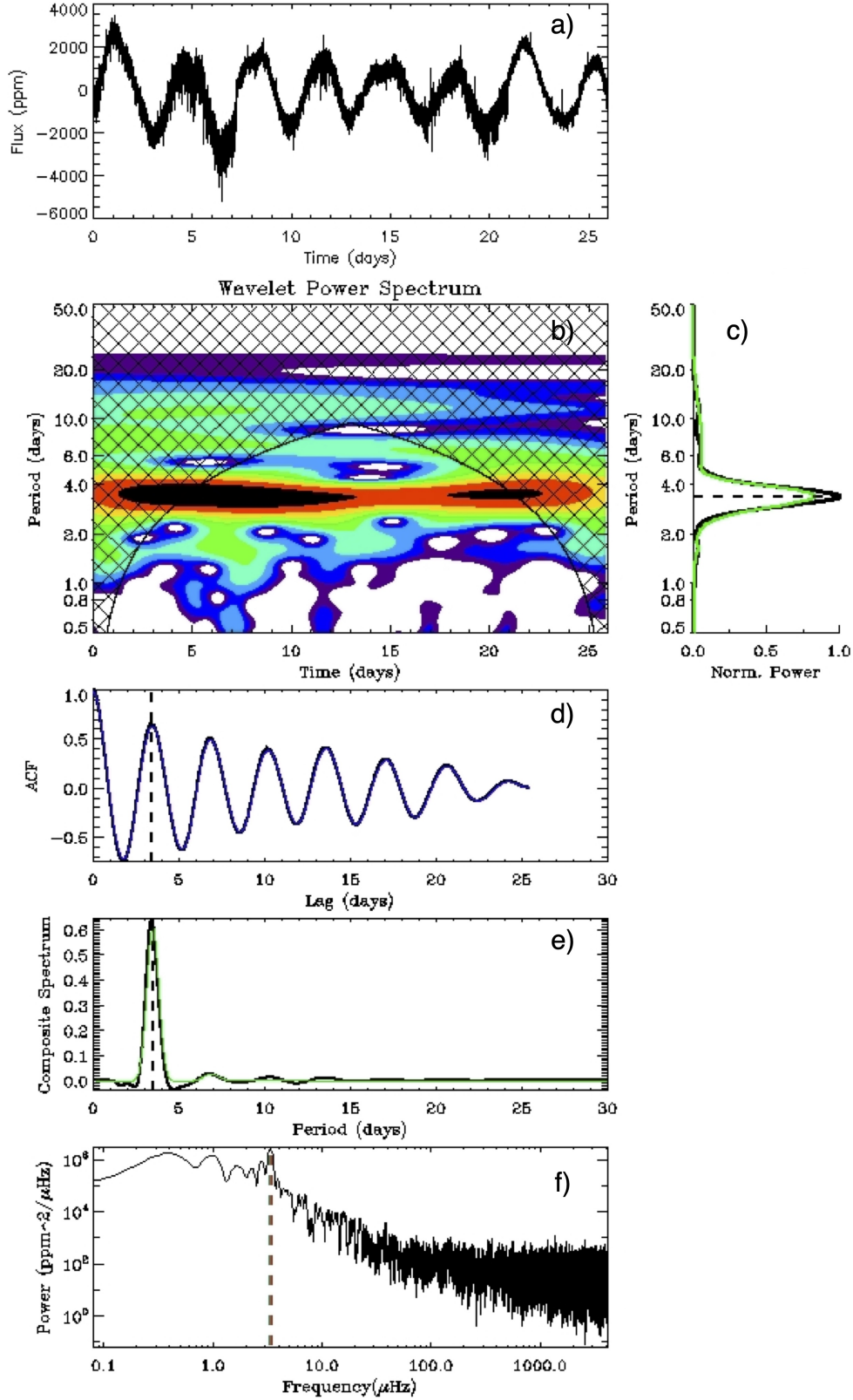


Figure 6. (a) TESS lightcurve for the rotation analysis. (b) Time-period analysis using wavelets. Black corresponds to high power and blue to low power. Black hatched area represents the region that cannot be sampled with the current length of the lightcurve. (c) Projection of the period-time analysis onto the period axis (black) and corresponding fits with multiple Gaussian functions (green). (d) Autocorrelation function. (e) Composite Spectrum (black) and best Gaussian fit (green). (f) PSD in logarithmic scale. The black dotted line indicates the rotation-period estimate.

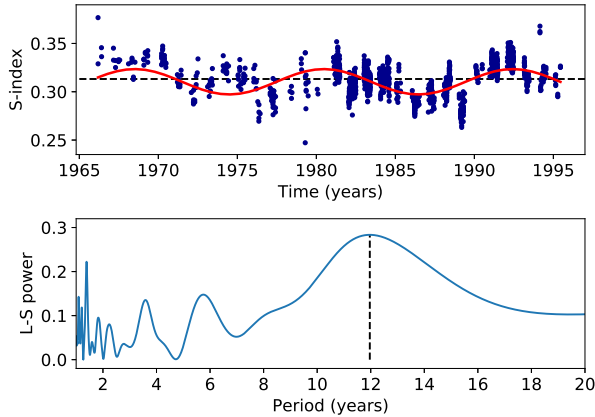


Figure 7. *Top panel:* Mount Wilson S-index measurements for the time interval 1966-1995. The dashed black line indicates the mean S-index. The red line shows the sinusoidal fit to the highest peak as provided by the periodogram in the bottom panel. *Bottom panel:* Lomb-Scargle periodogram of the S-index. The highest peak corresponds to a cycle period of $\approx 12 a$.

only has a SNR ~ 3 relative to the local background, so we would qualify this period as suggestive but not conclusive.

Given the short length of the TESS lightcurve, it is possible that the periodicity found of ≈ 3.4 years is a harmonic of the real P_{rot} , and the Mount Wilson period is indeed consistent with that interpretation. Longer high-quality time series would be necessary to conclude on the actual rotation period of this star.

4.2. Magnetic activity and cycles

While determining the magnetic activity level and the eventual presence of a periodic variability of a star (i.e., a stellar cycle), a key role is played by long-term datasets providing measurements of chromospheric proxies. As known from literature, many stars other than the Sun show a chromospheric variability related to magnetic activity which exhibit periodic variations (see e.g., Baliunas et al. 1995; Hall 2008). A periodic variability is typically visible also in the photospheric emission, whose phase difference with the chromospheric one reveals the activity dominant regime of the star, i.e. faculae-dominated (phase) or spot-dominated (anti-phase) (Radick et al. 1998; Reinhold et al. 2019). Before searching for the presence of a periodicity and to assess its level of magnetic activity, as in Sec. 4.1, we chose to discard the 3 outliers measurements in the following data analysis of the S-index.

In order to evaluate the magnetic activity level of the star, we firstly computed the average S-index over the whole time interval (1966-1995) as well as its extreme values. The data are shown in the top panel of Fig. 7. The mean S-index is 0.313, while the minimum and maximum values are respectively 0.247 and 0.377. If we compare the mean value

with the solar one for cycle 23 (0.170), as reported by Ege-land et al. (2017), we can infer that the mean MWO S-index of GJ 504 is around 1.8 times that of the Sun. In addition, the variability in the S-index (~ 0.13), i.e., the difference between the maximum and minimum values, is greater than that of the Sun during a solar cycle (~ 0.02). We are, therefore, facing a star whose chromospheric activity level is much higher with respect to that of a reference star like the Sun, pointing towards a probable age smaller than the solar one due to the fact that chromospheric activity typically decreases as the star evolves (Skumanich 1972; Mamajek & Hillenbrand 2008; Fabbian et al. 2017; Gondoin 2018).

To search for a long-term periodic variation, the observations of the S-index from the Mount Wilson Observatory available for a large number of stars, constitute a very useful tool. To do that we use an algorithm largely employed in astrophysics, the Lomb-Scargle periodogram (Lomb 1976; Scargle 1982) which, unlike the more classical Fourier analysis, allows to identify periodicity in unevenly sampled data, as in the case of the Mount Wilson observations. The computed Lomb-Scargle periodogram of GJ 504 is shown in the bottom panel of Fig. 7. Despite the presence of some peaks at small time scales (1.39, 3.59, and 5.75 a), partially due to the data sampling, the highest one corresponds to a main periodicity of 11.97 a. The corresponding false alarm probability (FAP) is $7.97 \cdot 10^{-93}$, indicating that the detected cycle period is statistically significant and unambiguous. This result indicates for this star the presence of a principal periodic chromospheric variability with a characteristic time quite similar to the Sun Schwabe 11-year cycle, even if it is set to a higher level of activity compared to the latter.

In addition to measuring the magnetic activity of GJ 504 with spectroscopic data, we also computed the photometric magnetic activity index, S_{ph} using TESS data. Following Mathur et al. (2014b,a), it is computed as the standard deviation of subseries of length $5 \times P_{\text{rot}}$ to ensure that we are measuring the variability due to the magnetic activity. From that temporal $S_{\text{ph}}(t)$, we take the mean value. Using the rotation period of 3.3 days found in Section 4.1, we obtain $S_{\text{ph}} = (1231 \pm 7.8)$ ppm.

5. SEARCHING FOR SOLAR-LIKE OSCILLATIONS

Based on the spectroscopic parameters of GJ 504, we looked for the solar-like oscillations using the prediction from Sects 2.3 and 2.4. As seen on Figure 5, the modes are not obvious and hence, we applied global seismic methods to look for the global seismic parameters.

In order to confirm the results obtained, the analysis of the power spectrum was independently performed by 4 teams who adopted different methods as described below.

The first method consisted in searching for the presence of oscillations in a region centered around 2000 μHz , as

suggested by the former predictions for ν_{\max} . For this purpose we adopted the public tool DIAMONDS³ (Corsaro & De Ridder 2014) coupled with the Background code extension⁴ for estimating the level of the background signal. The background signal, as described in Corsaro et al. (2017), comprises two Harvey-like profiles accounting for possible granulation-related signal and other variations at low frequency, a flat instrumental noise, and a Gaussian envelope of the solar-like oscillations. In particular we performed a Bayesian model comparison by means of the Bayesian evidence computed by DIAMONDS to select the best competing background model between one including the Gaussian envelope of the solar-like oscillations and one excluding it (see also Müllner et al. 2021). The resulting Bayes' factor suggests that the incorporation of an additional Gaussian profile is not statistically justified, meaning that in the light of the current data-set we could not detect the presence of a power excess due to stellar oscillations in this star. This result is depicted in Fig. 5, where no clear power excess due to stellar oscillations can be observed.

With the second method (applied to the second set of lightcurve), we searched for peaks in the resulting amplitude spectrum, requiring a minimum separation between peaks of 20 μHz , and generated an upper envelope across those peaks using cubic spline interpolation. The peak location of the resulting envelope, which represents ν_{\max} was estimated by fitting a Gaussian, and uncertainties in the resulting peak location estimated by a Monte Carlo simulation that allowed the minimum separation to vary between [0, 40] μHz . To estimate the large separation ν_{\max} , we performed an autocorrelation of the central 400 μHz of the amplitude spectrum, and used the Monte Carlo process to quantify the uncertainty in that estimate. This process resulted in $\nu_{\max} = 1919 \pm 40 \mu\text{Hz}$ and $\Delta\nu = 85.0 \pm 3.6 \mu\text{Hz}$. However, the peak envelope height is not large enough to claim statistical significance for this result, though it is suggestive and we will use this value for comparison with the theoretical models.

The third pulsation search algorithm is an upgraded version of Benomar et al. (2012) and was applied to the third lightcurve described in Section 3. The first step consists in getting initial guesses for a Bayesian analysis that follows if pulsations are detected conclusively. A first power spectrum F_{noise} of the star is produced by heavily smoothing (box-car smoothing of width $\approx 100 \mu\text{Hz}$) the original power spectrum. This allows to have an approximation of the noise background as pulsations (if any) are damped by the smoothing. A second spectrum F_{modes} is produced using a smoothing coefficient (box-car smoothing of $\approx 0.8 \mu\text{Hz}$) optimised for

revealing individual pulsations. The maximum of amplitude of the ratio $F_{\text{modes}}/F_{\text{noise}}$ is then estimated by performing a local 3rd order polynomial fit. The FWHM of the polynomial curve is used to have a first estimate of the potential region for pulsations and the Height-to-Noise ratio is used to evaluate the significance. We found only a marginal detection of pulsation at $\nu = 2040 \pm 282 \mu\text{Hz}$. To confirm the detection, a fit of the power spectrum is performed. It involves describing pulsations with a gaussian envelope and the noise background with two Harvey-like profiles (Harvey 1985) and white noise. Unfortunately, the Bayesian Maximum a Posteriori estimates gives us a significance for pulsations below 1% when compared to a pure noise fit of the spectrum.

Finally, another team analyzed two sets of lightcurves (LC1 and the one with our own aperture) with the A2Z pipeline (Mathur et al. 2010). Briefly, they looked for the mean large frequency spacing by computing the power spectrum of the power spectrum. We then fitted the background with three components: a Harvey law to model the granulation where the slope was fixed to 4, a Gaussian function for the modes and the white noise. After subtracting the background without the Gaussian function, we fitted another Gaussian function to estimate the frequency of the maximum power. A blind run of the A2Z pipeline finds some excess of power around 1000 μHz but no frequency spacing that agrees with the global seismic scaling relations (Kjeldsen & Bedding 1995) is measured with a high level of confidence level. By forcing the pipeline to look around 2000 μHz , a frequency spacing of $\sim 84 \mu\text{Hz}$ is measured with more than 95% confidence level but no Gaussian fit converged to obtain ν_{\max} . These results lead to a non detection of the modes with the A2Z pipeline.

6. DISCUSSION

6.1. Impact of magnetic activity on the solar-like oscillations

We discuss here the analysis of the TESS data and the non-detection of pulsation modes on the solar-like star GJ 504. While some hints of appearance of frequency spacing was found by the application of one of the methods, no reliable detection of solar-like oscillations can finally be reported. It is possible that this might be due to the high noise of the TESS data and the fact that only one sector was available. However, another possible explanation can be attributed to the presence of a high level of magnetic activity. In fact, several authors have already shown that magnetic activity is responsible for suppression of solar-like oscillations as already found in several targets (e.g. García et al. 2010; Chaplin et al. 2011b; Mathur et al. 2019b). The evolutionary stage, the estimate of the age and the analysis of the magnetic activity indexes of GJ 504 as developed in Sects. 4.2 reveal a level of magnetic activity typical of young solar-like objects (ref).

³ <https://github.com/EnricoCorsaro/DIAMONDS>

⁴ <https://github.com/EnricoCorsaro/Background>

In fact, the analysis of the chromospheric emission, through the S-index, has highlighted a fairly high level of magnetic activity (mean S-index = 0.313), ~ 1.8 times that of the Sun. The study of the periodicities with the Lomb-Scargle algorithm has pointed out a main principal cycle at 11.97 years, in agreement with the 11.79 ± 0.28 a detected cycle by Boro Saikia et al. (2018), but also revealed the presence of other smaller amplitude cycles. The coexistence of different cycles is a typical characteristic of fast rotating stars, where a higher number of dynamo modes are excited (Durney et al. 1981; Oláh et al. 2016), as it is the case of this star for which we found $P_{\text{rot}} \simeq 12.5$ days.

Once the stellar rotation and the main activity cycle period are known, we can compute the ratio $P_{\text{cyc}}/P_{\text{rot}}$, a quantity which is known to be related to the dynamo number N_D (see e.g., Soon et al. 1993; Baliunas et al. 1996). For stars older than 2.5 Gyrs, like the Sun, the quantity $\log(P_{\text{cyc}}/P_{\text{rot}})$ is typically around 2 (see Fig. 6 in Oláh et al. (2016)), while we obtain 2.54. This result indicates that GJ 504 is an active star with an age smaller than the one where the transition from spot to faculae domination, associated with a Rossby number ~ 1 and an age ~ 2.55 Gyr (Reinhold et al. 2019), is believed to happen. This is in agreement with our age estimation of 1.3 ± 1.3 Gyr. This is also consistent with the fact that Reinhold et al. (2019) found the photometric and chromospheric variability to be out of phase ($\Delta\phi = 0.34$), indicating that the star is still in the spot-dominated activity regime which characterize the young and active stars.

Concerning our attempt to detect solar-like pulsations, we used the calibrated formula by Bonanno et al. (2014), to relate the Mount-Wilson chromospheric S-index to the global oscillation amplitude A_{max} . By using the mean S-index obtained in Sect. 4.2, we obtain for this star a regime of significant oscillation amplitude suppression (see, e.g., Fig. 2 of Bonanno et al. 2014), defined by an expected global oscillation amplitude of $A_{\text{max}} = 1.6$ ppm, which is rather low as compared to the level of background found in the data. This magnetic activity suppression likely justifies the non-detection of an oscillation power excess in the stellar power spectrum. Even in the case of minimum of activity, corresponding to an S-index of 0.247 (see Sec. 4.2), the expected oscillation amplitude would be 2.6 ppm, which appears to be lower than the average background noise in the TESS data estimated to be 6.3 ppm from the background fitting we performed.

In addition, as obtained in Sect. 4.2, the S_{ph} of this star is (1231 ± 7.8) ppm during the TESS observations. Knowing that for the Sun, the average S_{ph} value is 166.1 ppm, we must conclude once more that GJ 504 appears to be very active (7.5 times higher than the Sun) in agreement with the result obtained from the spectroscopic observations. Comparing this level of activity with the stars with and without detection of

modes (see Figure 10 of Mathur et al. 2019a), only 3 stars with a detection of solar-like oscillations have an S_{ph} above 1000 ppm. For these stars, the comparison of the amplitude of the modes observed in the *Kepler* data and the predicted amplitude gives that $A_{\text{max,obs}}/A_{\text{max,pred}} \sim 0.8$ in average, varying between 0.70 and 0.93. This means that we can have a reduction from 7 to 30% in the amplitude of the modes. In the case that we are dominated by the noise, this can even add to the explanation of the non detection of the modes in this star. Note that these three *Kepler* stars are metal poor (with [Fe/H] around -0.2dex), which according to Samadi (2011) can lead to higher amplitudes and could counter-balance the effect of the surface magnetic activity.

6.2. Implication of the oscillatory behaviour on the age of GJ 504

In the attempt to better discern the most plausible stellar characteristics able to resemble GJ 504, it is possible to compare the properties of the oscillation frequencies calculated for the produced grid of theoretical models with the average properties, although uncertain, of the observed oscillation spectrum. Among all the calculated models, only Model 4 of Table 6.2 is able to reproduce within the errors the value of large separation found in Sec 5. We notice that models that reproduce this large separation seem to show values of $\log g$ and T_{eff} which lie nearly at the edges of the one-sigma error box (see Fig. 2).

The predicted oscillatory behaviour can be evinced from plots such as those shown in Figure 8, which reproduce the so called échelle diagrams obtained for Model 1 and Model 4 of Table , in which the oscillation frequencies are plotted as a function of the frequency modulo the large separation, and modes of low harmonic degree form roughly vertical ridges. The figures clearly show that models with small differences will show a different pattern of individual frequencies and hence have a well recognizable oscillatory behaviour, if the individual frequencies could have been detected.

It is very interesting to point out that models that match the SED luminosity, are characterized by a very young age ≤ 0.7 Gyr, while models which reproduce the provisional large separation 85.0 ± 3.6 show a more evolved structures with age above 2 Gyr and higher luminosity. It is clear that even just the measurement of the large separation, if confirmed, will definitely help to constrain the debated evolutionary state of this target and of its companion. But this will be achieved only with better conditions of signal to noise ratio (i. e., spectroscopic observations, smaller cadence mode etc....).

7. CONCLUSION

In this article we present a new attempt to study the solar-like star GJ 504, observed by the space mission TESS and

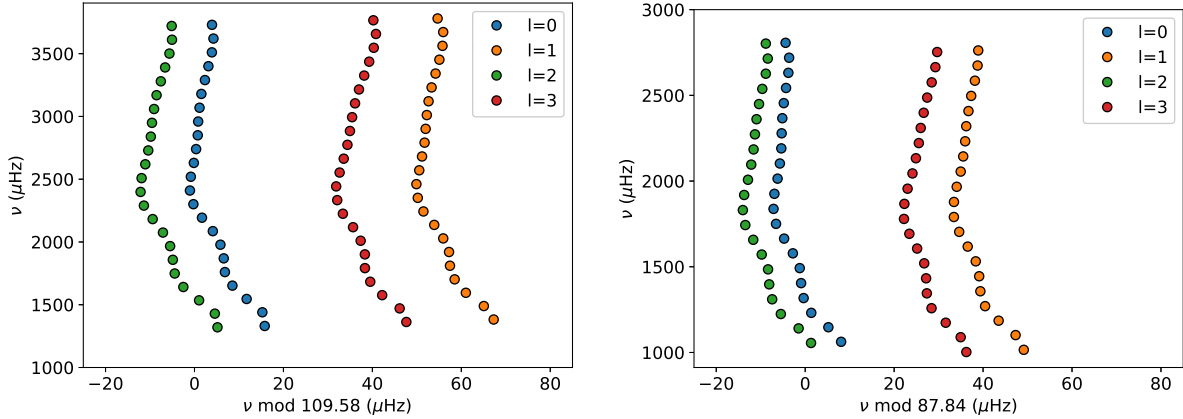


Figure 8. Echelle diagrams calculated for the two selected structure models: Model 1 (left panel) and Model 2 (right panel) of Table 6.2. Different colours are used to distinguish modes with different harmonic degrees.

Table 4. The parameters of GJ 504 as derived by the present analysis based on the use of TESS and Mount Wilson data.

	Present value
M/M_{\odot}	1.28 ± 0.07
Age (Gyr)	1.3 ± 1.3
R/R_{\odot}	1.38 ± 0.20
P_{rot} (d)	12.5 ± 2.8
S-index	0.313 ± 0.07
S_{ph} (ppm)	1231 ± 7.8
P_{cyc} (a)	11.97
$\Delta\nu$ (μHz)	85 ± 3.6
ν_{max} (μHz)	1919 ± 40

NOTE— M/M_{\odot} is the mass of the star, R/R_{\odot} is the surface radius, while P_{rot} and P_{cyc} are the surface rotation period and the activity cycle respectively. $\Delta\nu$ and ν_{max} are the dubious values of large separation and frequency of maximum amplitude of oscillation provided by the present analysis.

known to host an exoplanet with values of mass and radius not yet confirmed. Unfortunately, we did not succeed to characterize this star by means of asteroseismic techniques, since we did not find evidence for a clear excess of power, although a marginal detection of pulsations seems to manifest at about $\nu_{\text{max}} = 1919 \pm 40 \mu\text{Hz}$ with some indication of large separation with $\Delta\nu = (85 \pm 3.6) \mu\text{Hz}$. This non detection can be explained by the high level of magnetic activity for the star. Indeed the spectroscopic analysis yields an S-index of

0.313 and the photometric analysis of the TESS light curves provides a magnetic proxy S_{ph} of 1231 ppm, both indexes being much larger than the solar value of 0.170 and 161 ppm respectively. Given the values of the S-index and S_{ph} , the modes are predicted to suffer an important decrease of their amplitudes, probably close to the noise level in the TESS observations.

Nevertheless, all the results that we have deduced by analyzing the photometric data by the TESS space mission, supported by the measurements collected by the Mount Wilson Observatory long term campaign spanning nearly 30 years and by the modeling procedures have allowed us to get important conclusions on the large debated parameters of this target. In Table 4 we summarize the stellar parameters that best represent GJ 504.

Firstly, the analysis of the three decades long Mount Wilson spectroscopic observations yields the detection of a main magnetic cycle of 11.97-a and, at least, other two smaller amplitude cycles of 5.75 a and 3.59 a.

Further, the analysis of the Mount Wilson data allowed us to measure a stellar rotational period $P_{\text{rot}} = 12.5$ d, while the TESS light curves show a modulation of 3.3 d. Thus, we are able to conclude that it is very likely that the short length of one TESS sector leads to the measurement of a harmonic of the real rotational period.

The age of GJ 504, as obtained by stellar modelling based on accurate spectroscopic fundamental parameters, appears to be $\text{Age} \leq 2.6$ Gyr in agreement, within the quoted uncertainties, with the value of $2.5^{+1.0}_{-0.7}$ Gyr by D’Orazi et al. (2017). In particular, the rotational period and the main magnetic cycle locate this G-type star in the regime of chromospheric activity dominated by the superposition of several magnetic cycles during which, as shown by van Saders et al. (2016) and Metcalfe & van Saders (2017), the magnetic braking is still in act while the rotation is slowing down. This situation put this target well before the magnetic transi-

tion, which will bring this star at the age of about 4-5 Gyr to the shutdown of the magnetic braking reaching a low activity state.

Adopting this new age value, along with SPHERE JHK_1K_2 photometry for the companion (Bonnetfoy et al. 2018) and the COND-AMES model atmospheres (Baraffe et al. 2003), we gather companion mass and radius of $M_{GJ504b} = (16.5 \pm 4.8)M_{Jup}$ and $R_{GJ504b} = (1.00 \pm 0.03)R_{Jup}$ (the related errors are simply the standard deviation from the four photometric bands, so they are certainly underestimated). Hence, given the large uncertainty in age, we cannot confirm/disprove from the present study whether GJ504b is located in the brown dwarf or planetary regime.

Future observations of this target with a 20-second cadence might reduce the level of noise as shown for instance by Huber et al. (2021) and might allow us to detect the excess of power due to oscillations. In particular, considering the measured period of the main magnetic cycle, it might be better to observe again this star during the magnetic minimum, which should occur between 2022 and 2023. Thus, GJ 504 is scheduled to be re-observed with TESS in Sector 50 with 20-second cadence mode. Based on its TESS magnitude, 20-second cadence data should yield an improvement in photometric precision of $\approx 30\%$ due to the reduced influence of pointing jitter on cosmic-ray rejection for bright stars (Huber et al. 2022). This improved precision may allow the detection of oscillations.

For the future, we believe that GJ 504 might represent an ideal target also for the ESA/PLATO (Rauer et al. 2016) space mission, with scheduled launch in the end of

2026, having the potential with its high-precision, high-time-resolution and high-duty-cycle photometry to detect individual oscillation frequencies in this star, leading finally not only to clarify the evolutionary state of this system but also to solve hot questions related to the use of rotation and magnetic activity as a diagnostic of stellar age and finally leading to a clear and more accurate concept of gyrochronology.

The publication of the present article has been supported by INAF through the Main-Stream call 2018-‘Stellar evolution and pulsations in the context of the PLATO space mission’. This paper includes data collected with the TESS mission, obtained from the MAST data archive at the Space Telescope Science Institute (STScI). Funding for the TESS mission is provided by the NASA Explorer Program. STScI is operated by the Association of Universities for Research in Astronomy, Inc., under NASA contract NAS 5–26555. R.A.G. acknowledges funding from the PLATO CNES grant. S.M. acknowledges support by the Spanish Ministry of Science and Innovation with the Ramon y Cajal fellowship number RYC-2015-17697 and the grant number PID2019-107187GB-I00. D.B. acknowledges support from the National Aeronautics and Space Administration under the Living With A Star program, grant number NNX16AB76G. R.R. is a PhD student of the PhD course in Astronomy, Astrophysics and Space Science, a joint research program between the University of Rome ‘Tor Vergata’, the Sapienza University of Rome and the National Institute of Astrophysics (INAF).

REFERENCES

- Addison, B. C., Wright, D. J., Nicholson, B. A., et al. 2021, *MNRAS*, 502, 3704, doi: [10.1093/mnras/staa3960](https://doi.org/10.1093/mnras/staa3960)
- Angulo, C., Arnould, M., Rayet, M., et al. 1999, *NuPhA*, 656, 3, doi: [10.1016/S0375-9474\(99\)00030-5](https://doi.org/10.1016/S0375-9474(99)00030-5)
- Baglin, A., Auvergne, M., Boisnard, L., et al. 2006, in 36th COSPAR Scientific Assembly, Vol. 36, 3749
- Baliunas, S. L., Nesme-Ribes, E., Sokoloff, D., & Soon, W. H. 1996, *ApJ*, 460, 848, doi: [10.1086/177014](https://doi.org/10.1086/177014)
- Baliunas, S. L., Donahue, R. A., Soon, W. H., et al. 1995, *ApJ*, 438, 269, doi: [10.1086/175072](https://doi.org/10.1086/175072)
- Baraffe, I., Chabrier, G., Barman, T. S., Allard, F., & Hauschildt, P. H. 2003, *A&A*, 402, 701, doi: [10.1051/0004-6361/20030252](https://doi.org/10.1051/0004-6361/20030252)
- Barnes, S. A. 2007, *ApJ*, 669, 1167, doi: [10.1086/519295](https://doi.org/10.1086/519295)
- Battistini, C., & Bensby, T. 2015, *A&A*, 577, A9, doi: [10.1051/0004-6361/201425327](https://doi.org/10.1051/0004-6361/201425327)
- Beck, P. G., Montalbán, J., Kallinger, T., et al. 2012, *Nature*, 481, 55, doi: [10.1038/nature10612](https://doi.org/10.1038/nature10612)
- Bedding, T. R. 2014, in *Asteroseismology*, ed. P. L. Pallé & C. Esteban, 60
- Bedding, T. R., & Kjeldsen, H. 2003, *PASA*, 20, 203, doi: [10.1071/AS03025](https://doi.org/10.1071/AS03025)
- Bedding, T. R., Mosser, B., Huber, D., et al. 2011, *Nature*, 471, 608, doi: [10.1038/nature09935](https://doi.org/10.1038/nature09935)
- Belkacem, K., Goupil, M. J., Dupret, M. A., et al. 2011, *A&A*, 530, A142, doi: [10.1051/0004-6361/201116490](https://doi.org/10.1051/0004-6361/201116490)
- Benomar, O., Baudin, F., Chaplin, W., Elsworth, Y., & Appourchaux, T. 2012, *mnras*, 420, 2178, doi: [10.1111/j.1365-2966.2011.20184.x](https://doi.org/10.1111/j.1365-2966.2011.20184.x)
- Böhm-Vitense, E. 1958, *ZA*, 46, 108
- Bonanno, A., Corsaro, E., & Karoff, C. 2014, *A&A*, 571, A35, doi: [10.1051/0004-6361/201424632](https://doi.org/10.1051/0004-6361/201424632)
- Bonnetfoy, M., Perraut, K., Lagrange, A. M., et al. 2018, *A&A*, 618, A63, doi: [10.1051/0004-6361/201832942](https://doi.org/10.1051/0004-6361/201832942)
- Boro Saikia, S., Marvin, C. J., Jeffers, S. V., et al. 2018, *A&A*, 616, A108, doi: [10.1051/0004-6361/201629518](https://doi.org/10.1051/0004-6361/201629518)

- 966 Borucki, W. J., Koch, D., Basri, G., et al. 2010, *Science*, 327, 977,
967 doi: [10.1126/science.1185402](https://doi.org/10.1126/science.1185402)
- 968 Borucki, W. J., Agol, E., Fressin, F., et al. 2013, *Science*, 340, 587,
969 doi: [10.1126/science.1234702](https://doi.org/10.1126/science.1234702)
- 970 Brown, T. M., Gilliland, R. L., Noyes, R. W., & Ramsey, L. W.
971 1991, *ApJ*, 368, 599, doi: [10.1086/169725](https://doi.org/10.1086/169725)
- 972 Buzasi, Derek, L., Carboneau, L., Hessler, C., Lezcano, A., &
973 Preston, H. 2016, *IAU Focus Meeting*, 29B, 673,
974 doi: [10.1017/S1743921316006335](https://doi.org/10.1017/S1743921316006335)
- 975 Campante, T. L., Schofield, M., Kuszlewicz, J. S., et al. 2016, *ApJ*,
976 830, 138, doi: [10.3847/0004-637X/830/2/138](https://doi.org/10.3847/0004-637X/830/2/138)
- 977 Ceillier, T., van Saders, J., García, R. A., et al. 2016, *MNRAS*,
978 456, 119, doi: [10.1093/mnras/stv2622](https://doi.org/10.1093/mnras/stv2622)
- 979 Chaplin, W. J., Houdek, G., Appourchaux, T., et al. 2008, *A&A*,
980 485, 813, doi: [10.1051/0004-6361/200809695](https://doi.org/10.1051/0004-6361/200809695)
- 981 Chaplin, W. J., Kjeldsen, H., Bedding, T. R., et al. 2011a, *ApJ*, 732,
982 54, doi: [10.1088/0004-637X/732/1/54](https://doi.org/10.1088/0004-637X/732/1/54)
- 983 Chaplin, W. J., Bedding, T. R., Bonanno, A., et al. 2011b, *ApJL*,
984 732, L5, doi: [10.1088/2041-8205/732/1/L5](https://doi.org/10.1088/2041-8205/732/1/L5)
- 985 Chaplin, W. J., Sanchis-Ojeda, R., Campante, T. L., et al. 2013,
986 *ApJ*, 766, 101, doi: [10.1088/0004-637X/766/2/101](https://doi.org/10.1088/0004-637X/766/2/101)
- 987 Chontos, A., Huber, D., Kjeldsen, H., et al. 2020, arXiv e-prints,
988 arXiv:2012.10797. <https://arxiv.org/abs/2012.10797>
- 989 Christensen-Dalsgaard, J. 1988, in *Advances in Helio- and*
990 *Asteroseismology*, ed. J. Christensen-Dalsgaard & S. Frandsen,
991 Vol. 123, 295
- 992 Christensen-Dalsgaard, J. 2008a, *Ap&SS*, 316, 13,
993 doi: [10.1007/s10509-007-9675-5](https://doi.org/10.1007/s10509-007-9675-5)
- 994 —. 2008b, *Ap&SS*, 316, 113, doi: [10.1007/s10509-007-9689-z](https://doi.org/10.1007/s10509-007-9689-z)
- 995 Corsaro, E., & De Ridder, J. 2014, *A&A*, 571, A71,
996 doi: [10.1051/0004-6361/201424181](https://doi.org/10.1051/0004-6361/201424181)
- 997 Corsaro, E., Mathur, S., García, R. A., et al. 2017, *A&A*, 605, A3,
998 doi: [10.1051/0004-6361/201731094](https://doi.org/10.1051/0004-6361/201731094)
- 999 da Silva, R., Porto de Mello, G. F., Milone, A. C., et al. 2012,
1000 *A&A*, 542, A84, doi: [10.1051/0004-6361/201118751](https://doi.org/10.1051/0004-6361/201118751)
- 1001 Donahue, R. A., Saar, S. H., & Baliunas, S. L. 1996, *ApJ*, 466,
1002 384, doi: [10.1086/177517](https://doi.org/10.1086/177517)
- 1003 D’Orazi, V., Desidera, S., Gratton, R. G., et al. 2017, *A&A*, 598,
1004 A19, doi: [10.1051/0004-6361/201629283](https://doi.org/10.1051/0004-6361/201629283)
- 1005 Durney, B. R., Mihalas, D., & Robinson, R. D. 1981, *PASP*, 93,
1006 537, doi: [10.1086/130878](https://doi.org/10.1086/130878)
- 1007 Egeland, R., Soon, W., Baliunas, S., et al. 2017, *ApJ*, 835, 25,
1008 doi: [10.3847/1538-4357/835/1/25](https://doi.org/10.3847/1538-4357/835/1/25)
- 1009 Fabbian, D., Simoniello, R., Collet, R., et al. 2017, *Astronomische*
1010 *Nachrichten*, 338, 753, doi: [10.1002/asna.201713403](https://doi.org/10.1002/asna.201713403)
- 1011 Fuhrmann, K. 2004, *Astronomische Nachrichten*, 325, 3,
1012 doi: [10.1002/asna.200310173](https://doi.org/10.1002/asna.200310173)
- 1013 Fuhrmann, K., & Chini, R. 2015, *ApJ*, 806, 163,
1014 doi: [10.1088/0004-637X/806/2/163](https://doi.org/10.1088/0004-637X/806/2/163)
- 1015 Gaia Collaboration. 2018, *VizieR Online Data Catalog*, I/345
- 1016 Gandolfi, D., Barragán, O., Livingston, J. H., et al. 2018, *A&A*,
1017 619, L10, doi: [10.1051/0004-6361/201834289](https://doi.org/10.1051/0004-6361/201834289)
- 1018 García, R. A., & Ballot, J. 2019, *Living Reviews in Solar Physics*,
1019 16, 4, doi: [10.1007/s41116-019-0020-1](https://doi.org/10.1007/s41116-019-0020-1)
- 1020 García, R. A., Mathur, S., Salabert, D., et al. 2010, *Science*, 329,
1021 1032, doi: [10.1126/science.1191064](https://doi.org/10.1126/science.1191064)
- 1022 García, R. A., Hekker, S., Stello, D., et al. 2011, *MNRAS*, 414, L6,
1023 doi: [10.1111/j.1745-3933.2011.01042.x](https://doi.org/10.1111/j.1745-3933.2011.01042.x)
- 1024 García, R. A., Mathur, S., Pires, S., et al. 2014a, *A&A*, 568, A10,
1025 doi: [10.1051/0004-6361/201323326](https://doi.org/10.1051/0004-6361/201323326)
- 1026 García, R. A., Ceillier, T., Salabert, D., et al. 2014b, *A&A*, 572,
1027 A34, doi: [10.1051/0004-6361/201423888](https://doi.org/10.1051/0004-6361/201423888)
- 1028 Gaulme, P., Jackiewicz, J., Spada, F., et al. 2020, *A&A*, 639, A63,
1029 doi: [10.1051/0004-6361/202037781](https://doi.org/10.1051/0004-6361/202037781)
- 1030 Gondoin, P. 2018, *A&A*, 616, A154,
1031 doi: [10.1051/0004-6361/201731541](https://doi.org/10.1051/0004-6361/201731541)
- 1032 Grevesse, N., & Noels, A. 1993, in *Origin and Evolution of the*
1033 *Elements*, ed. N. Prantzos, E. Vangioni-Flam, & M. Casse,
1034 15–25
- 1035 Hall, J. C. 2008, *Living Reviews in Solar Physics*, 5, 2,
1036 doi: [10.12942/lrsp-2008-2](https://doi.org/10.12942/lrsp-2008-2)
- 1037 Harvey, J. 1985, *ESA SP*, 235, 199
- 1038 Huber, D., Bedding, T. R., Stello, D., et al. 2011, *ApJ*, 743, 143,
1039 doi: [10.1088/0004-637X/743/2/143](https://doi.org/10.1088/0004-637X/743/2/143)
- 1040 Huber, D., Chaplin, W. J., Christensen-Dalsgaard, J., et al. 2013,
1041 *ApJ*, 767, 127, doi: [10.1088/0004-637X/767/2/127](https://doi.org/10.1088/0004-637X/767/2/127)
- 1042 Huber, D., Chaplin, W. J., Chontos, A., et al. 2019, *AJ*, 157, 245,
1043 doi: [10.3847/1538-3881/ab1488](https://doi.org/10.3847/1538-3881/ab1488)
- 1044 Huber, D., White, T. R., Metcalfe, T. S., et al. 2021, arXiv e-prints,
1045 arXiv:2108.09109. <https://arxiv.org/abs/2108.09109>
- 1046 —. 2022, *AJ*, 163, 79, doi: [10.3847/1538-3881/ac3000](https://doi.org/10.3847/1538-3881/ac3000)
- 1047 Iglesias, C. A., & Rogers, F. J. 1996, *ApJ*, 464, 943,
1048 doi: [10.1086/177381](https://doi.org/10.1086/177381)
- 1049 Janson, M., Brandt, T. D., Kuzuhara, M., et al. 2013, *ApJL*, 778,
1050 L4, doi: [10.1088/2041-8205/778/1/L4](https://doi.org/10.1088/2041-8205/778/1/L4)
- 1051 Jenkins, J. M., Twicken, J. D., McCauliff, S., et al. 2016, in *Society*
1052 *of Photo-Optical Instrumentation Engineers (SPIE) Conference*
1053 *Series*, Vol. 9913, *Software and Cyberinfrastructure for*
1054 *Astronomy IV*, ed. G. Chiozzi & J. C. Guzman, 99133E,
1055 doi: [10.1117/12.2233418](https://doi.org/10.1117/12.2233418)
- 1056 Jones, E., Oliphant, T., Peterson, P., et al. 2001, *SciPy: Open*
1057 *source scientific tools for Python*. <http://www.scipy.org/>
- 1058 Kiefer, R., Schad, A., Davies, G., & Roth, M. 2017, *A&A*, 598,
1059 A77, doi: [10.1051/0004-6361/201628469](https://doi.org/10.1051/0004-6361/201628469)
- 1060 Kjeldsen, H., & Bedding, T. R. 1995, *A&A*, 293, 87,
1061 <https://arxiv.org/abs/astro-ph/9403015>
- 1062 Kjeldsen, H., Bedding, T. R., Arentoft, T., et al. 2008, *ApJ*, 682,
1063 1370, doi: [10.1086/589142](https://doi.org/10.1086/589142)
- 1064 Kuzuhara, M., Tamura, M., Kudo, T., et al. 2013, *ApJ*, 774, 11,
1065 doi: [10.1088/0004-637X/774/1/11](https://doi.org/10.1088/0004-637X/774/1/11)

- 1066 Lebreton, Y., & Goupil, M. J. 2014, *A&A*, 569, A21,
1067 doi: [10.1051/0004-6361/201423797](https://doi.org/10.1051/0004-6361/201423797)
- 1068 Lebreton, Y., Goupil, M. J., & Montalbán, J. 2014, in *EAS*
1069 *Publications Series*, Vol. 65, *EAS Publications Series*, 177–223,
1070 doi: [10.1051/eas/1465005](https://doi.org/10.1051/eas/1465005)
- 1071 Lomb, N. R. 1976, *Ap&SS*, 39, 447, doi: [10.1007/BF00648343](https://doi.org/10.1007/BF00648343)
- 1072 Maldonado, J., Eiroa, C., Villaver, E., Montesinos, B., & Mora, A.
1073 2015, *A&A*, 579, A20, doi: [10.1051/0004-6361/201525764](https://doi.org/10.1051/0004-6361/201525764)
- 1074 Mamajek, E. E., & Hillenbrand, L. A. 2008, *ApJ*, 687, 1264,
1075 doi: [10.1086/591785](https://doi.org/10.1086/591785)
- 1076 Mathur, S., García, R. A., Bugnet, L., et al. 2019a, *Frontiers in*
1077 *Astronomy and Space Sciences*, 6, 46,
1078 doi: [10.3389/fspas.2019.00046](https://doi.org/10.3389/fspas.2019.00046)
- 1079 —. 2019b, *Frontiers in Astronomy and Space Sciences*, 6, 46,
1080 doi: [10.3389/fspas.2019.00046](https://doi.org/10.3389/fspas.2019.00046)
- 1081 Mathur, S., Salabert, D., García, R. A., & Ceillier, T. 2014a,
1082 *Journal of Space Weather and Space Climate*, 4, A15,
1083 doi: [10.1051/swsc/2014011](https://doi.org/10.1051/swsc/2014011)
- 1084 Mathur, S., García, R. A., Régulo, C., et al. 2010, *A&A*, 511, A46,
1085 doi: [10.1051/0004-6361/200913266](https://doi.org/10.1051/0004-6361/200913266)
- 1086 Mathur, S., García, R. A., Ballot, J., et al. 2014b, *A&A*, 562, A124,
1087 doi: [10.1051/0004-6361/201322707](https://doi.org/10.1051/0004-6361/201322707)
- 1088 McQuillan, A., Mazeh, T., & Aigrain, S. 2014, *ApJS*, 211, 24,
1089 doi: [10.1088/0067-0049/211/2/24](https://doi.org/10.1088/0067-0049/211/2/24)
- 1090 Mermilliod, J. C. 2006, *VizieR Online Data Catalog*, II/168
- 1091 Messina, S., Pizzolato, N., Guinan, E. F., & Rodonò, M. 2003,
1092 *A&A*, 410, 671, doi: [10.1051/0004-6361:20031203](https://doi.org/10.1051/0004-6361:20031203)
- 1093 Metcalfe, T. S., & van Saders, J. 2017, *SoPh*, 292, 126,
1094 doi: [10.1007/s11207-017-1157-5](https://doi.org/10.1007/s11207-017-1157-5)
- 1095 Metcalfe, T. S., Monteiro, M. J. P. F. G., Thompson, M. J., et al.
1096 2010, *ApJ*, 723, 1583, doi: [10.1088/0004-637X/723/2/1583](https://doi.org/10.1088/0004-637X/723/2/1583)
- 1097 Metcalfe, T. S., van Saders, J. L., Basu, S., et al. 2020, *ApJ*, 900,
1098 154, doi: [10.3847/1538-4357/aba963](https://doi.org/10.3847/1538-4357/aba963)
- 1099 —. 2021, *ApJ*, 921, 122, doi: [10.3847/1538-4357/ac1f19](https://doi.org/10.3847/1538-4357/ac1f19)
- 1100 Mishenina, T. V., Pignatari, M., Korotin, S. A., et al. 2013, *A&A*,
1101 552, A128, doi: [10.1051/0004-6361/201220687](https://doi.org/10.1051/0004-6361/201220687)
- 1102 Müllner, M., Zwintz, K., Corsaro, E., et al. 2021, *A&A*, 647,
1103 A168, doi: [10.1051/0004-6361/202039578](https://doi.org/10.1051/0004-6361/202039578)
- 1104 Nielsen, M. B., Ball, W. H., Standing, M. R., et al. 2020, *arXiv*
1105 *e-prints*, arXiv:2007.00497
- 1106 Oláh, K., Kóvári, Z., Petrovay, K., et al. 2016, *A&A*, 590, A133,
1107 doi: [10.1051/0004-6361/201628479](https://doi.org/10.1051/0004-6361/201628479)
- 1108 Paunzen, E. 2015, *VizieR Online Data Catalog*, J/A+A/580/A23
- 1109 Pires, S., Mathur, S., García, R. A., et al. 2015, *A&A*, 574, A18,
1110 doi: [10.1051/0004-6361/201322361](https://doi.org/10.1051/0004-6361/201322361)
- 1111 Radick, R. R., Lockwood, G. W., Skiff, B. A., & Baliunas, S. L.
1112 1998, *ApJS*, 118, 239, doi: [10.1086/313135](https://doi.org/10.1086/313135)
- 1113 Ramírez, I., Allende Prieto, C., & Lambert, D. L. 2013, *ApJ*, 764,
1114 78, doi: [10.1088/0004-637X/764/1/78](https://doi.org/10.1088/0004-637X/764/1/78)
- 1115 Rauer, H., Aerts, C., Cabrera, J., & PLATO Team. 2016,
1116 *Astronomische Nachrichten*, 337, 961,
1117 doi: [10.1002/asna.201612408](https://doi.org/10.1002/asna.201612408)
- 1118 Reinhold, T., Bell, K. J., Kuzlewicz, J., Hekker, S., & Shapiro,
1119 A. I. 2019, *A&A*, 621, A21, doi: [10.1051/0004-6361/201833754](https://doi.org/10.1051/0004-6361/201833754)
- 1120 Ricker, G. R., Winn, J. N., Vanderspek, R., et al. 2014, in *Society*
1121 *of Photo-Optical Instrumentation Engineers (SPIE) Conference*
1122 *Series*, Vol. 9143, *Space Telescopes and Instrumentation 2014:*
1123 *Optical, Infrared, and Millimeter Wave*, ed. J. Oschmann,
1124 Jacobus M., M. Clampin, G. G. Fazio, & H. A. MacEwen,
1125 914320, doi: [10.1117/12.2063489](https://doi.org/10.1117/12.2063489)
- 1126 Rogers, F. J., & Nayfonov, A. 2002, *ApJ*, 576, 1064,
1127 doi: [10.1086/341894](https://doi.org/10.1086/341894)
- 1128 Samadi, R. 2011, *Stochastic Excitation of Acoustic Modes in*
1129 *Stars*, ed. J.-P. Rozelot & C. Neiner, Vol. 832, 305,
1130 doi: [10.1007/978-3-642-19928-8_11](https://doi.org/10.1007/978-3-642-19928-8_11)
- 1131 Santos, A. R. G., Breton, S. N., Mathur, S., & García, R. A. 2021,
1132 *ApJS*, 255, 17, doi: [10.3847/1538-4365/ac033f](https://doi.org/10.3847/1538-4365/ac033f)
- 1133 Santos, A. R. G., García, R. A., Mathur, S., et al. 2019, *ApJS*, 244,
1134 21, doi: [10.3847/1538-4365/ab3b56](https://doi.org/10.3847/1538-4365/ab3b56)
- 1135 Santos, A. R. G., Campante, T. L., Chaplin, W. J., et al. 2018,
1136 *ApJS*, 237, 17, doi: [10.3847/1538-4365/aac9b6](https://doi.org/10.3847/1538-4365/aac9b6)
- 1137 Scargle, J. D. 1982, *ApJ*, 263, 835, doi: [10.1086/160554](https://doi.org/10.1086/160554)
- 1138 Schofield, M., Chaplin, W. J., Huber, D., et al. 2019, *ApJS*, 241,
1139 12, doi: [10.3847/1538-4365/ab04f5](https://doi.org/10.3847/1538-4365/ab04f5)
- 1140 Silva Aguirre, V., Davies, G. R., Basu, S., et al. 2015, *MNRAS*,
1141 452, 2127, doi: [10.1093/mnras/stv1388](https://doi.org/10.1093/mnras/stv1388)
- 1142 Skemer, A. J., Morley, C. V., Zimmerman, N. T., et al. 2016, *ApJ*,
1143 817, 166, doi: [10.3847/0004-637X/817/2/166](https://doi.org/10.3847/0004-637X/817/2/166)
- 1144 Skumanich, A. 1972, *ApJ*, 171, 565, doi: [10.1086/151310](https://doi.org/10.1086/151310)
- 1145 Soderblom, D. R., Hillenbrand, L. A., Jeffries, R. D., Mamajek,
1146 E. E., & Naylor, T. 2014, in *Protostars and Planets VI*, ed.
1147 H. Beuther, R. S. Klessen, C. P. Dullemond, & T. Henning, 219,
1148 doi: [10.2458/azu_uapress_9780816531240-ch010](https://doi.org/10.2458/azu_uapress_9780816531240-ch010)
- 1149 Soon, W. H., Baliunas, S. L., & Zhang, Q. 1993, *ApJL*, 414, L33,
1150 doi: [10.1086/186989](https://doi.org/10.1086/186989)
- 1151 Stassun, K. G., Collins, K. A., & Gaudi, B. S. 2017, *AJ*, 153, 136,
1152 doi: [10.3847/1538-3881/aa5df3](https://doi.org/10.3847/1538-3881/aa5df3)
- 1153 Stassun, K. G., Corsaro, E., Pepper, J. A., & Gaudi, B. S. 2018, *AJ*,
1154 155, 22, doi: [10.3847/1538-3881/aa998a](https://doi.org/10.3847/1538-3881/aa998a)
- 1155 Stassun, K. G., & Torres, G. 2016, *AJ*, 152, 180,
1156 doi: [10.3847/0004-6256/152/6/180](https://doi.org/10.3847/0004-6256/152/6/180)
- 1157 —. 2021, *ApJL*, 907, L33, doi: [10.3847/2041-8213/abdaad](https://doi.org/10.3847/2041-8213/abdaad)
- 1158 Stassun, K. G., Oelkers, R. J., Paegert, M., et al. 2019, *AJ*, 158,
1159 138, doi: [10.3847/1538-3881/ab3467](https://doi.org/10.3847/1538-3881/ab3467)
- 1160 Stello, D., Bruntt, H., Preston, H., & Buzasi, D. 2008, *The*
1161 *Astrophysical Journal*, 674, L53, doi: [10.1086/528936](https://doi.org/10.1086/528936)
- 1162 Stello, D., Cantiello, M., Fuller, J., et al. 2016, *Nature*, 529, 364,
1163 doi: [10.1038/nature16171](https://doi.org/10.1038/nature16171)
- 1164 Tassoul, M. 1980, *ApJS*, 43, 469, doi: [10.1086/190678](https://doi.org/10.1086/190678)

- 1165 Torrence, C., & Compo, G. P. 1998, *Bulletin of the American*
1166 *Meteorological Society*, 79, 61,
1167 doi: [10.1175/1520-0477\(1998\)079](https://doi.org/10.1175/1520-0477(1998)079)
- 1168 Torres, G., Andersen, J., & Giménez, A. 2010, *A&A Rv*, 18, 67,
1169 doi: [10.1007/s00159-009-0025-1](https://doi.org/10.1007/s00159-009-0025-1)
- 1170 Valenti, J. A., & Fischer, D. A. 2005, *ApJS*, 159, 141,
1171 doi: [10.1086/430500](https://doi.org/10.1086/430500)
- 1172 Van Eylen, V., Lund, M. N., Silva Aguirre, V., et al. 2014, *ApJ*,
1173 782, 14, doi: [10.1088/0004-637X/782/1/14](https://doi.org/10.1088/0004-637X/782/1/14)
- 1174 van Saders, J. L., Ceillier, T., Metcalfe, T. S., et al. 2016, *Nature*,
1175 529, 181, doi: [10.1038/nature16168](https://doi.org/10.1038/nature16168)
- 1176 Vaughan, A. H., Preston, G. W., & Wilson, O. C. 1978, *PASP*, 90,
1177 267, doi: [10.1086/130324](https://doi.org/10.1086/130324)
- 1178 Wilson, O. C. 1968, *ApJ*, 153, 221, doi: [10.1086/149652](https://doi.org/10.1086/149652)
- 1179 —. 1978, *ApJ*, 226, 379, doi: [10.1086/156618](https://doi.org/10.1086/156618)
- 1180 Wright, D. J., Chené, A.-N., De Cat, P., et al. 2011, *ApJL*, 728,
1181 L20, doi: [10.1088/2041-8205/728/1/L20](https://doi.org/10.1088/2041-8205/728/1/L20)